Experiment-based simulation of a cross-flow large-scale SOFC model

Zhonghui Song[1], Xingyu Xiong[1, *], Liming Ba[2] and Kao Liang[1]

[1] School of Energy, Power and Mechanical Engineering, North China Electric Power University, Beijing, China
[2] School of Chemical & Environment Engineering, China University of Mining and Technology-Beijing, Beijing, 100083, China

Abstract. The multi-physical field full-coupling simulation of solid oxide fuel cell (SOFC) stack requires huge computational resources. Repeated iteration of highly non-linear calculation is easy to cause oscillation and lead to solution failure. At present, the simulation of SOFC stack models mainly focuses on the co-flow condition and counter-flow condition models. Most of them are simplified models that simplify the stack scale or physical field. In this paper, a SOFC decoupling model based on machine learning is established, and the full three-dimensional and multi-physical fields of the cross-flow large-scale SOFC stack are simulated. The model is divided into three parts for calculation, unit cell model, alternative mapping model, and cross-flow large-scale SOFC stack model. The alternative mapping model obtained by the BP neural network algorithm replaces the nonlinear multi-physics equations in the traditional model. Compared with the traditional method, the decoupling model can greatly reduce the computing resources and improve the stability of computing. In this paper, the experimental data of the single cell and the 30-layer stack are used to calibrate and verify the simulation results of stack. Studying the performance of the SOFC stack under different parameter conditions. Temperature, flow uniformity, gas mole fraction, and voltage distribution in the SOFC stack under different inlet flow rates and stack currents are obtained. Obtaining the output power and fuel utilization rate of the stack under different working conditions.

Keywords: Cross-flow large scale SOFC model; Multi physical field coupling; BP neural networks.

1. Introduction

Solid oxide fuel cell is a device that directly converts the chemical energy of fuel into electrical energy. Compared with other fuel cells, solid oxide fuel cell (SOFC) is recognized for its high efficiency, high fuel flexibility, elimination of expensive catalysts and integration with bottom cycle / cogeneration system [1-3]. However, the large-scale commercial application of SOFC is difficult to achieve. This is because SOFC has a complex operating environment and high temperature, about700~1000℃, which is used to maintain the high oxygen ion conductivity of solid oxide electrolyte [4]. Moreover, SOFC structure is small, and the experimental method will be very expensive and time-consuming. It is difficult to directly measure the details of chemicals, current and potential in the SOFC [4, 5].In order to understand the internal situation of the SOFC, you need to simulate and analyze the battery stack. In recent years, many scholars have simulated SOFC. M. Peksen et al. [6] studied the 36-layer counter-flow condition SOFC stack, carried out three-dimensional fluid-thermal coupling analysis. The nonlinear elastic-plastic behavior of interconnect plates is considered in the study of coupled computational mechanics, and the position vulnerable to stress in SOFC stack is determined. Zhao et al. [7] studied the flow distribution and pressure change of 40-layer SOFC, explained the influence of manifold connection position, size and tube number on flow uniformity, and used it to optimize the design parameters of external manifold. Jawad Hussain et al. [8] established a three-dimensional model of single channel, carried out multi physical field simulation, and studied the performance parameters of SOFC.N. Russner et al. [9] studied the single-layer co-flow condition SOFC model, compared the different SOFC structures, the different electrical losses generated by Anode supported cells(ASC) and electrolyte supported cells (ESC), resulting in different temperature distribution in SOFC stack. Ma et al. [10] used the unsteady two-dimensional model based on COMSOL software to study the carbon deposition process in planar SOFC and the mechanism of carbon deposition in SOFC under different operating time was analyzed. Chen et al. [11] established solid oxide fuel cell The numerical model of (SOFC) button cell focuses on the influence of finger channel on the gas transport process in anode support. The mole fraction distribution, diffusion flux and convection flux of H_2 in porous layer are discussed in detail. Su et al.

* Corresponding author: Xingyu.xiong@ncepu.edu.cn

[12]studied and solved the shortcomings of SOFC related to thin electrode, proposed anode-cathode-supported SOFC (ACSC), and established the mathematical model of anode supported SOFC (ASC) and ACSC. The model captured the complex interdependence between charge and gas transport and electrochemical reaction. S.-S. Wei et al. [13] established a three-layer counter-flow condition SOFC stack model, proposed a new channel and stack layout design, considered the influence of channel design on stack performance, and analyzed the thermal stress of planar anode supported solid oxide fuel cell stack. E. Birgersson et al. [14] Simplified the three-dimensional fuel cell model into two-dimensional by combining spatial smoothing and progressive analysis. In the flow field composed of parallel plane channels and solid ribs, the spatial smooth energy equation is established according to local thermal equilibrium (LTE) and local thermal nonequilibrium (LTNE) conditions. Min Yan et al. [15] Proposed a new spiral SOFC interconnect, which can realize tight gas sealing, and achieve sufficient electrical contact between the interconnect and the electrode or gas supply pipeline, thus alleviating the fuel shortage of planar SOFC porous electrode. From the above research, it can be seen that most of the research on SOFC is highly simplified models, including plane two-dimensional model, single channel model or single-layer cell model, and the complex multi-physical field coupling of the SOFC is simplified to a single physical field. There is a lack of simulation and experimental verification, and the accuracy and reliability of the simulation model are insufficient. This is bound to make the simulation results can't well reflect the actual operation of the SOFC. At present, the simulation of SOFC stack models mainly focuses on the co-flow condition and counter-flow condition models. There are few multi-physical field simulations for cross-flow condition large-scale SOFC stacks. Using the decoupling method, the multi-physical field coupling model of large-scale SOFC stack is divided into three parts to calculate, unit cell model, alternative mapping model and stack model. Finally, the simulation results of cross-flow condition SOFC coupled with multiple-physical fields are obtained. Compared with the experiment to verify the accuracy and reliability of the simulation model.

2. Model

2.1 Mathematical model

2.1.1 Electrochemical model.

The electromotive force (EMF), also known as Nernst ideal potential, is determined by the change of Gibbs free energy of electrochemical reaction. The total electromotive force of the reaction is expressed by Nernst equation [16]:

$$E_{Nernst} = E^0 + \frac{RT}{2F}\ln\left(\frac{P_{H_2}P_{O_2}{}^{1/2}}{P_{H_2O}}\right) = -\frac{\Delta G^0}{2F} + \frac{RT}{2F}\ln\left(\frac{P_{H_2}P_{O_2}{}^{1/2}}{P_{H_2O}}\right) \quad (1)$$

Where E^0 is the standard Nernst electromotive force, which is the Nernst electromotive force when the temperature is T and the partial pressures of hydrogen, water vapor and oxygen are all standard pressures.ΔG^0 is the standard Gibbs free energy, R is the general gas constant, $Jmol^{-1}K^{-1}$, F is the Faraday constant.

During the actual operation of SOFC, polarization loss will occur, resulting in that the output voltage of the cell is less than Nernst electromotive force, and the output voltage of the cell is:

$$V_{cell} = E_0 - \eta_{conc}^{an} - \eta_{conc}^{ca} - \eta_{ohm,an} - \eta_{ohm,ca} - \eta_{ohm,ele} - \eta_{act,an} - \eta_{act,ca} \quad (2)$$

Where, E_0 is Nernst electromotive force; $\eta_{conc}^{an}, \eta_{conc}^{ca}$ are the concentration polarization potential of anode and cathode respectively; $\eta_{act,an}, \eta_{act,ca}$ are the active polarization potentials of anode and cathode respectively; $\eta_{ohm,an}, \eta_{ohm,ca}, \eta_{ohm,ele}$ are the ohmic losses of anode, cathode and electrolyte respectively.

Activation polarization potential η_{act} is not described by explicit equation. Generally, its relationship with current density is described by Bulter-Volmer equation:

$$i = i_0\left[\frac{C_R^*}{C_R^{0^*}}e^{\frac{\alpha_1 nF\eta}{RT}} - \frac{C_P^*}{C_p^{0^*}}e^{-\frac{\alpha_2 nF\eta}{RT}}\right] \quad (3)$$

Where α_1, α_2 is the transfer coefficient, i_0 is the exchange current density and i is the local current density.

The concentration polarization formula is:

$$\eta_{conc}^{an} = \frac{RT}{2F}\ln\left(\frac{p_{H_2}}{P_{H_2O}}\right) - \frac{RT}{2F}\ln\left(\frac{p_{H_2}}{P_{H_2O}}\right) \quad (4)$$

$$\eta_{conc}^{ca} = \frac{RT}{4F}\ln\left(\frac{pO_2}{p^0}\right) - \frac{RT}{4F}\ln\left(\frac{pO_2}{p^0}\right) \quad (5)$$

Where, p represents the pressure of each component and p^0 represents the standard condition pressure.

Ohmic polarization is the polarization caused by ohmic resistance, including voltage loss caused by resistance of electrolyte, cathode, anode and connector. Moreover, because electrons migrate by potential difference and ions transition in oxygen holes by concentration difference. The loss of ohmic polarization caused by ion conduction accounts for the main part. The materials of porous anode, dense electrolyte and porous cathode are Ni / YSZ, YSZ and LSM / YSZ respectively.

Ohmic polarization is calculated by Ohm's Law:

$$\eta_{ohm} = R_{tot}i \quad (6)$$

R_{tot} is the total surface resistance, which can be calculated by the following formula [17]:

$$R_{tot} = \left[\left(\frac{\delta_{ele,a}}{\sigma_{ele,a}}\right) + \left(\frac{\delta_{ion}}{\sigma_{ion}}\right) + \left(\frac{\delta_{ele,c}}{\sigma_{ele,c}}\right)\right] \quad (7)$$

Where $\delta_{ele,a}, \delta_{ele,c}$ and δ_{ion} represents the thickness of anode, cathode and electrolyte respectively. $\sigma_{ele,a}$, $\sigma_{ele,c}$ represents the electronic conductivity of the anode and cathode electrodes, respectively, σ_{ion} is the ionic conductivity of the electrolyte.

2.1.2 Mass transport model.

The material transfer of mixed gas in the gas channel and porous electrode region includes convection and diffusion [18]. The continuity equation for mixtures containing n gases is expressed as [5]:

$$\frac{\partial(\varphi\rho)}{\partial t} + \sum_{k=1}^{n} \nabla \cdot M_k j_k = \sum_{k=1}^{n} S_k \quad (8)$$

Where, ρ is the density of the gas mixture, φ is porous electrode pore, n is the number of gases, j_k, M_k and S_k are the molecular flux, molecular mass and mass source rate of the species,S_k Calculation formula of S_k[6,19,20].

Anode fuel gas and cathode air are the mixture of two gases. The influence of porosity is not considered in the channel. The diffusion process can be described by Maxwell-Stefan model (MSM). The binary diffusion coefficient of MSM model is expressed as:

$$D_{kl} = \frac{3.198\times10^{-8}T^{1.75}}{p\left(v_k^{1/3}+v_l^{1/3}\right)^2}\left(\frac{1}{M_k}+\frac{1}{M_l}\right)^{0.5} \quad (9)$$

Where M_k and M_l are the molar mass of substance k(l), V_k and V_l are the diffusion volume of substance k(l). For hydrogen, water, oxygen and nitrogen, their values are respectively: $6.12\times10^{-6}, 13.1\times10^{-6}, 16.3\times10^{-6}, 18.5\times10^{-6} m^3/mol$.

The gas diffusion in the porous electrode area adopts the dust gas model (DGM), and the diffusion coefficient of the porous medium is as follows:

$$D_k^{eff} = \frac{D_{kl}^{eff} D_{kKn}^{eff}}{D_{kl}^{eff} + x_k D_{kl}^{eff} + x_l D_{kKn}^{eff}} \quad (10)$$

Where x_k, x_l are the mole fraction of substance k (l) , $D_{kl}^{eff}, D_{kKn}^{eff}$ are the effective binary diffusion coefficient and the effective Knudsen diffusion coefficient of substance i respectively,$D_{kl}^{eff}, D_{kKn}^{eff}$ can be expressed by the following formula [21]:

The general form of mass conservation equation is:

$$\nabla J_k^m = \nabla(-\rho D_k \nabla w_k + \rho w_k u) = S \quad (11)$$

Where, J_k^m is the mass flow of substance k;D_k is the diffusion coefficient of substance k ; w_k is the mass fraction of substance k;S is mass source term, whose size is as follows according to charge conservation:

$$S_{H_2} = -\frac{i}{2F} M_{H_2} \quad (12)$$

$$S_{H_2O} = \frac{i}{2F} M_{H_2O} \quad (13)$$

$$S_{O_2} = -\frac{i}{4F} M_{O_2} \quad (14)$$

2.1.3 Energy model.

There are two heat transfer mechanisms in SOFC: heat conduction in porous media region and convective heat transfer in fluid region (ignoring radiation heat transfer). The heat transfer in porous media is based on the assumption of local heat balance and the governing equation of energy conservation [22]:

$$\rho C_p u \cdot \nabla T + \nabla \cdot (-\lambda_{eff} \nabla T) = Q_h \quad (15)$$

Where the first term is the convective heat transfer term in the fluid region; The second term is the heat conduction term in the fluid region and the porous medium region; Q_h is the energy source term, $W \cdot m^{-3}$, ρ is the density of the gas mixture, $kg \cdot m^{-3}$, C_p is the specific constant pressure heat capacity of the gas mixture, $J \cdot kg^{-1} \cdot K^{-1}$, u is the velocity field determined by momentum transfer,$m \cdot s^{-1}$, λ_{eff} is the effective thermal conductivity, $W \cdot m \cdot K^{-1}$.

2.2 Unit cell model

The planar SOFC stack is composed of single cells with the same structure. The single cell is composed of repeated units of the flow channel, and the unit cell model is a part of the flow channel. Unit cell has a complete electrochemical reaction and material transfer process. In this paper, COMSOL is used to establish the cross-flow condition unit cell model. The size of the unit cell model is very small, which is 22.528 mm2. The structure of the unit cell model is shown in Fig.1 and the simulation parameters of the model are shown in Table 1:

The initial conditions of the unit cell model are shown in Table 2:

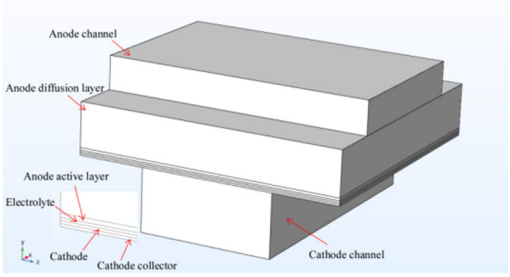

Figure 1. Unit cell model structure

Table 1. Model parameters

Item	Value	Unit
Height of anode flow channel	0.4	mm
Width of anode flow channel	2	mm
Width of anode flow channel rib	1	mm
Height of cathode flow channel	0.75	mm
Width of cathode flow channel	1.6	mm
Width of Cathode flow channel rib	1.6	mm
Thickness of anode diffusion layer	0.53	mm
Thickness of anode function layer	0.03	mm
Thickness of electrolyte	0.02	mm
Thickness of cathode function layer	0.02	mm
Porosity in anode ε_a	0.4	
Porosity in cathode ε_c	0.3	
Anode specific surface area	1.5e6	1/m
Cathode specific surface area	1.1e6	1/m
Anode permeability	1e-9	m^2
Cathode permeability	1e-9	m^2
Operation pressure P	1	atm

Table 2. Initial conditions of unit model

Item	Value	Unit
Anode flow rate	0.2	L/min
Cathode flow rate	0.4	L/min
H_2 inlet mass fraction	0.782	
O_2 inlet mass fraction	0.233	

The unit cell model calculates the working conditions with inlet temperatures of 973.15 K, 1023.15 K and 1073.15 K, and compares the simulated I-V curve with the experimental data of button SOFC to verify the accuracy and reliability of the model.

2.3 30-layer stack model

The 30-layer cross-flow condition SOFC stack model is stacked by unit cell models. The the 30-layer cross-flow condition SOFC stack model structure is shown in Fig.2:

2.4 Parametric calculation

These unit cell models composed of cross-flow condition channels can be spliced into a complete SOFC stack model. Reasonable design of the operating conditions of the unit cell model can describe all the operating conditions in the SOFC stack. Reasonable setting of parameter scanning range to calculate the unit cell model can save computing resources while ensuring comprehensive and accurate. The parameterization of unit cell model can be set from the following parameters: temperature, output voltage, inlet H_2 mass fraction and inlet O_2 mass fraction. There are 4800 small cases with different parameter combinations. Extract the results of parametric calculation. Each source item has 772800 pairs of data. Modeling for alternative mapping model. Parameter information is listed in Table 3:

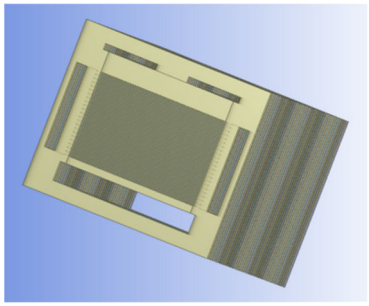

Figure 2. 30-layer cross-flow condition SOFC stack structure

Table 3. Parametric calculation scheme design

Item	Start point	End point	Levels
Anode H_2 mass content	0.782	0.079	20
Cathode O_2 mass content	0.233	0.1124	10
Temperature	973.15k	1073.15k	6
Voltage	0.6	0.9	4

2.5 Alternative mapping model

The alternative mapping model is the adhesive between the unit cell model coupled with multiple physical fields and the SOFC stack model. The results of the parametric calculation of the unit cell model are trained by the machine learning algorithm to obtain a linear equation related to the parameters, so as to replace the combination of the above highly nonlinear physical equations. This linear equation is used to solve the subsequent 30-layer SOFC large stack model.

This paper uses BP neural network algorithm to establish alternative mapping model. BP neural network uses the error back propagation between the predicted value and the actual value to update the weight and threshold in the neural network. The relationship between input parameters and output values can be expressed as [23]:

$$y = f(\sum wx + b) \tag{16}$$

Where w is the weight, b is the threshold, x is the input parameter, and f is the activation function.

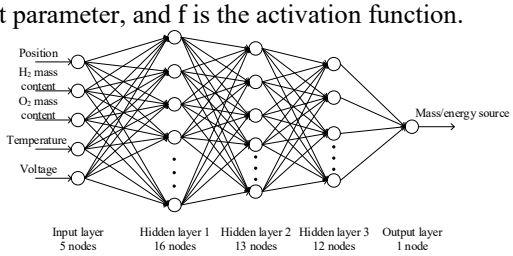

Figure 3. Structure diagram of BP neural network

The structure of BP neural network in this paper is 5-16-13-12-1, As shown in Fig.3. The activation function of the hidden layer is tansig function, and the activation function of the output layer is purelin function:

$$f(x) = \frac{2}{1+e^{-2x}} - 1 \tag{17}$$

In this paper, five BP neural network models are obtained, which are anode mass source, anode energy source, cathode mass source, cathode energy source and electrolyte energy source model. In order to improve the generalization ability of the model, the source item data is divided into two parts: training data and test data .Taking the anode mass source BP neural network model as an example, 75% of the 772800 pairs of data are used as the training data and 25% as the test data.

The BP neural network model selected in this paper has high prediction accuracy, and the relative errors are within ± 2%, the data with relative error within ± 1% accounted for 99.84%. The data points with large relative error are distributed at the very low H_2 reaction rate in the anode functional layer, which will not have a significant impact on the accuracy of the model. The fitting reliability (R) of BP neural network is better than 0.99999, and the root mean square error (RMSE) is 1.09e-5. The prediction error diagram of neural network is shown in Fig.4.Take the prediction model of anode mass source as an example:

3. Experiment

In this paper, two experiments are completed, the experimental data are collected as the basis for the reliability of the simulation model results. The structure, initial conditions and boundary conditions of the simulation model are consistent with the experiment. The first experiment is button SOFC experiment, and the second experiment is 30-layer SOFC stack experiment.

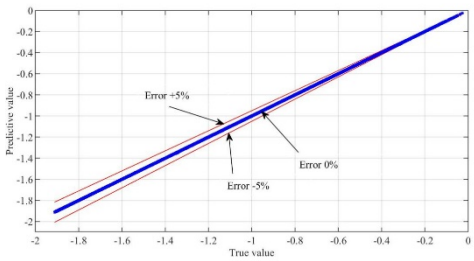

Figure 4. Prediction error of anode mass source BP neural network

Fig.5 shows the schematic diagram of the SOFC stack experimental device.

Taking the SOFC stack experiment as an example, it shows that 30-layer SOFC stack are put in a heating furnace equipped with thermocouples in order to control the operating temperature of the stack. The experimental fuel gas is hydrogen, which is provided by the hydrogen tank, and the cathode gas is oxygen, which is provided by the air compressor. The gas is preheated in the preheater and then connected to the reactor.

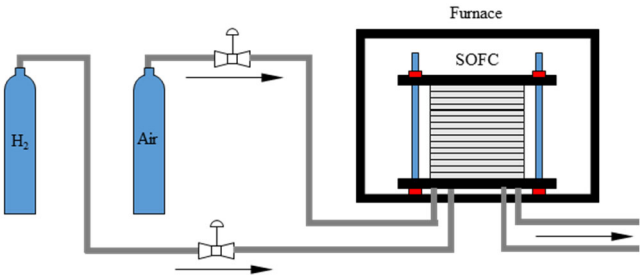

Figure 5. Schematic diagram of experiment

3.1 Experimental design

The experimental design includes four variables: furnace temperature, hydrogen flow rate, air flow rate and current. The detailed experimental scheme is shown in Table 4. The experiment completes the measurement of all parameter combinations, records the experimental data, and draws the I-V curve of the SOFC stack.

3.2 Experimental data acquisition

Raise the temperature of the heating furnace to the set temperature and wait for the temperature to stabilize. After the temperature is stable, the hydrogen and air in the gas preheater are put into the SOFC stack and reach the set value. This process should be carried out slowly in stages to avoid impact on the SOFC stack and affecting the experimental measurement. After the above operations are completed, start to run the measurement program for data acquisition.

Table 4. Experimental scheme design

furnace temperature (℃)	Air flow rate (L/min)	H_2 flow rate (L/min)	Current (A)
700	70	8.96	0→30
725	90	10.45	
750	100	12.54	

4. Results and discussion

4.1 Experimental verification

Compared with the experimental SOFC stack, the flow channel structure, initial conditions and boundary conditions inside the SOFC stack are consistent with those used in the experiment.

The first experiment is the button SOFC experiment, which is used to compare with the unit cell model simulation. Fig.6 shows the comparison of I-V curve of the unit cell model and button SOFC experiment. At inlet temperature of 1023.15K, when the output voltage is between 0.6V to 1V, the error is - 2.6% to 1.25%, and when the temperature condition is changed to 1073.15K, within the same output voltage range, the error is - 2.67% to 1.25%.

The second experiment is the 30-layer SOFC stack experiment, which is used to compare with the 30-layer SOFC stack simulation. Fig.7 shows the I-V curve comparison between the SOFC stack experiment and the SOFC stack simulation. At the inlet temperature of 1023.15K, when the experimental current is changed from 10A to 30A, the output voltage changes from 29.13V to 24.43V. Under the same conditions, when the simulation current is changed from 10A to 30A, the output voltage changes from 29.33V to 24.49V. The error range is -0.628% to 0.686%. When the experimental current changes from 10A to 30A at 998.15K inlet temperature, the output voltage changes from 29.03V to 24V. Under the same conditions, when the simulation current changes from 10A to 30A, the output voltage changes from 29.05V to 24V. The error ranges from-1.43% to 0.7%.

Through the comparison of experimental and simulation results, it can be seen that the results of the simulation model are accurate and reliable. The unit cell model is calculated in COMSOL, the number of grids is 20000, and the calculation time of each case is about 10s. BP neural network is trained in MATLAB. The training time of each anode source term and electrolyte source term is about 260s, and that of each cathode source term is slightly longer, about 1200s. Calculate the 30-layer SOFC stack model in fluent, and the number of grids is 9.5e7, and the calculation time of each working condition is about 7h.

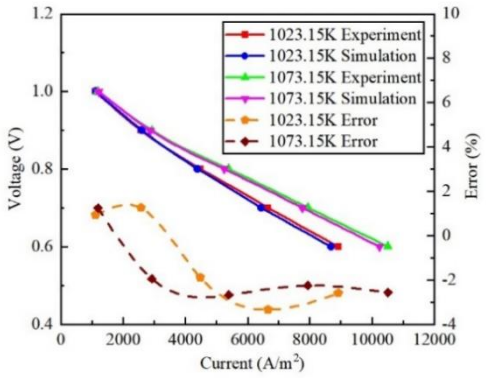

Figure 6. Comparison of I-V curve between unit cell model and button cell

4.2 Parameter distribution of inner stacks

4.2.1 Flow and Temperature

This paper takes the simulation results under the operating conditions of 1023.15k as an example. In the 30-layer cross-flow condition SOFC stack model, because the gas flow rates of different layers of cell and different flow channels are different, the gas distribution in the SOFC stack is uneven. In this paper the flow uniformity at the outlet of anode channel at the bottom of stack is 97.57%, and the flow uniformity at the outlet of anode channel at the top of stack is 96.37%.

Fig.8 shows the distribution of anode H_2 mole fraction under the conditions of inlet temperature is 1023.15K, H_2 inlet flow rate is 10.45 L/min and stack reference current is 25A. The X direction is the H_2 flow direction and the Z direction is the O_2 flow direction. It can be seen that the molar concentration of H_2 decreases gradually in the direction of H_2 flow, indicating that H_2 is consumed.

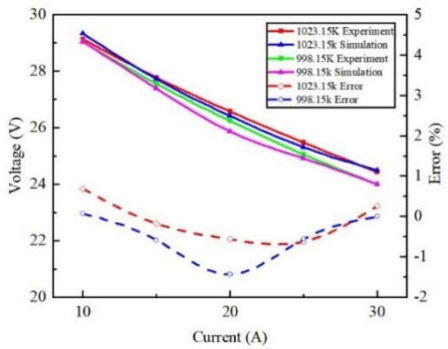

Figure 7. I-V curve comparison diagram of 30-layer stack

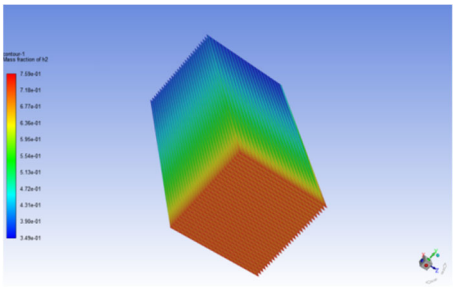

Figure 8. Anode H_2 mole fraction distribution

Fig.9 shows the temperature distribution of anode channel and gas distribution cavity under the conditions of inlet temperature 1023.15K, H_2 inlet flow rate 10.45 L/min and stack reference current 25A. The temperature increases gradually along the gas flow direction, and the maximum temperature is 1106K, which is located near the anode H_2 outlet and cathode O_2 outlet. And the temperature continues to accumulate with the gas flow, resulting in a gradual increase in the temperature along the gas flow direction.

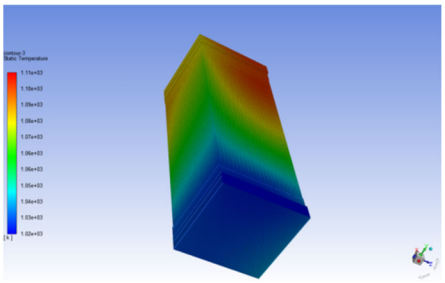

Figure 9. Anode H_2 temperature distribution

Fig.10 shows the average temperature of the gas in the cathode and anode channels in the 1st, 10th, 20th and 30th layers of SOFC stack. The gas temperature in the anode channel is higher than that in the cathode channel. This is because the heat generated by the reaction is taken away with the flow of excess cathode gas. Therefore, in the actual operation of the SOFC stack, the common method to reduce the temperature in the SOFC stack is to inject excess air into the cathode channel. Combine Fig.9 with fig.10 (a) and 10 (b). In the height direction of SOFC stack, the temperature of the bottom layer of the stack is higher than that of the top layer, which is caused by gas flow. In SOFC, the flowing gas is the main carrier of heat energy and determines the temperature distribution in the stack. In the process of flowing from the top to the bottom, it continuously absorbs the heat of the passing battery layer and accumulates the heat when flowing to the bottom. Therefore, the temperature at the bottom of the stack is higher than that at the top.

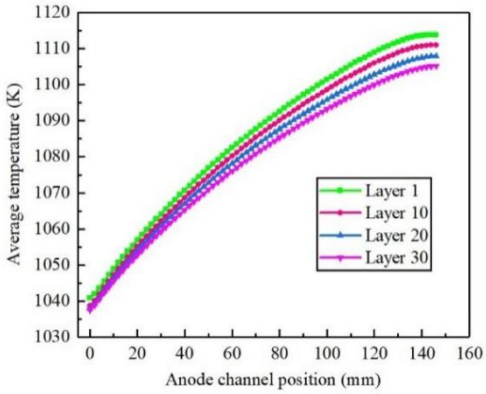

(a) Average anode gas temperature

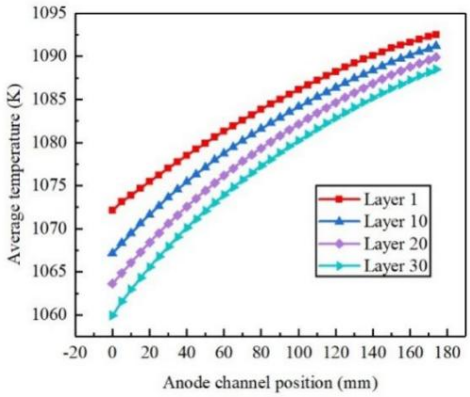

(b) Average temperature of cathode gas

Figure 10. Average gas temperature in cathode and anode channels of different layers of SOFC stack

Fig.11 shows the average temperature of SOFC stack anode gas under the conditions of inlet temperature is 1023.15K, H_2 inlet flow rate is 10.45 L/min and SOFC stack current is 20A, 25A and 30A.It can be seen from the figure that the gas temperature in the SOFC stack increases with the increase of current. At different stack currents, the temperature curve also changes. At 20A stack current, the temperature change increases monotonically in the direction of the flow channel. At 30A stack current, the temperature at the end of the channel decreases because the heat generation rate of gas reaction in the channel is greater than the gas heat transfer rate at 20A stack current, so the temperature continues to rise in the channel. At 25A and 30A stack current, the concentration of reaction gas in the channel decreases rapidly due to the fast gas reaction rate. At the end of the flow channel, the reaction gas concentration is very low, resulting in the gas reaction heat generation rate is lower than the heat conductivity, and the temperature decreases after reaching the peak.

4.2.2 Voltages

Fig.12 shows the relationship between the cell voltages of each layer in the SOFC stack under different stack currents. The analysis shows that the voltage distribution of each cell layer in SOFC stack is determined by the gas distribution and temperature distribution with each cell layer in the stack. As shown in Fig.12, under the same stack current, the cell voltage of each layer in the stack is not equal, and the voltage of each layer gradually decreases from the bottom layer of the stack to the top layer of the stack. Under different stack currents, the voltage difference between the cells in the stack increases with the increase of stack current. In other words, the greater the stack current, the greater the voltage difference between the cells in the stack. The voltage distribution between cell layers in SOFC stack is the result of the joint action of gas flow distribution and temperature distribution. In the 30-layer SOFC stack model used in this paper, the bottom gas flow rate is greater than the top gas flow rate, and the bottom cell temperature is also higher than the top cell temperature. The greater the gas flow rate and the higher the temperature, the faster the gas reaction rate, the greater the generated current and the higher the output power. Therefore, when the cell current of each layer is equal, the cell voltage at the bottom of the stack is higher than that at the top of the stack, and the output power at the bottom of the stack is higher. At a large stack current, the more obvious the performance difference between the cell layers, the lower the output voltage is bound to reduce the average output power of the SOFC stack and affect the performance of the SOFC stack.

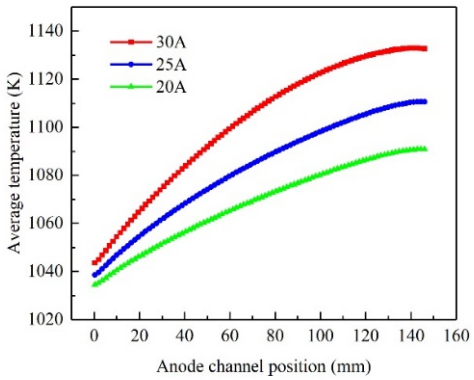

Figure 11. Average temperature of anode gas channel under different stack current

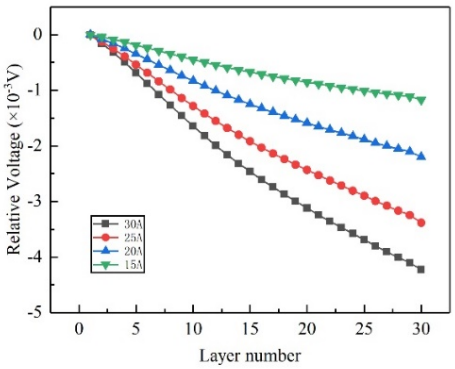

Figure 12. Voltage relationship between layers in stack under different stack currents

5. Conclusions

In this paper, the decoupling method is used to successfully solve the large-scale cross-flow condition SOFC stack model. Its multi-physical and multi-dimensional characteristics are described. The structure is optimized to improve the performance of SOFC stack. This method greatly shortens the calculation time and reduces the calculation resources. One working condition of unit cell model takes about 10s, and the calculation time of each working condition of large-scale stack is about 7h.

By comparing the I-V curves of simulation and experiment, it shows that the simulation model is accurate and reliable. Comparison between unit cell model and button cell experiment: When the inlet temperature is 1023.15K and the output voltage change range is 0.6V~1V, the error is -2.6%~1.25%. The temperature condition is changed to 1073.15K, within the same output voltage range, the error is -2.67%~1.25%. Experimental comparison between 30-layer stack model and 30-layer actual stack: At 1023.15K inlet temperature, changing the stack current from 10A to 30A, the error range is -0.628%~0.686%. At 998.15K inlet temperature, changing the stack current from 10A to 30A, the error range is -1.43%~0.7%.

The study found that the temperature in the cross-flow condition SOFC stack presents a wave-shaped distribution, the highest temperature appears near the anode and cathode gas channel outlets, and the temperature at the bottom of the stack is higher than the temperature at the top of the stack.

References

1. Li Y, Pang Y, Tu H, Torrigino F, Biollaz SMA, Li Z, et al. Impact of syngas from biomass gasification on solid oxide fuel cells: A review study for the energy transition. ENERG CONVERS MANAGE. 2021; 250:114894.
2. Kim DH, Bae Y, Lee S, Son J, Shim JH, Hong J. Thermal analysis of a 1-kW hydrogen-fueled solid oxide fuel cell stack by three-dimensional numerical simulation. ENERG CONVERS MANAGE. 2020; 222:113213.
3. Yuan J, Rokni M, Sundén B. Three-dimensional computational analysis of gas and heat transport phenomena in ducts relevant for anode-supported solid oxide fuel cells. INT J HEAT MASS TRAN. 2003; 46:809-21.
4. Wang Y, Yoshiba F, Watanabe T, Weng S. Numerical analysis of electrochemical characteristics and heat/species transport for planar porous-electrode-supported SOFC. J POWER SOURCES. 2007; 170:101-10.
5. Ba L, Xiong X, Yang Z, Lei Z, Ge B, Peng S. A novel multi-physics and multi-dimensional model for solid oxide fuel cell stacks based on alternative mapping of BP neural networks. J POWER SOURCES. 2021; 500:229784.
6. Peksen M. A coupled 3D thermofluid-thermomechanical analysis of a planar type production scale SOFC stack. INT JHYDROGEN ENERG. 2011; 36:11914-28.
7. Zhao C, Yang J, Zhang T, Yan D, Pu J, Chi B, et al. Numerical simulation of flow distribution for external manifold design in solid oxide fuel cell stack. INT J HYDROGEN ENERG. 2017; 42:7003-13.
8. Hussain J, Ali R, Akhtar MN, Jaffery MH, Shakir I, Raza R. Modeling and simulation of planar SOFC to study the electrochemical properties. CURR APPL PHYS. 2020; 20:660-72.
9. Russner N, Dierickx S, Weber A, Reimert R, Ivers-Tiffée E. Multiphysical modelling of planar solid oxide fuel cell stack layers. J POWER SOURCES. 2020; 451:227552.
10. Ma T, Yan M, Zeng M, Yuan J, Chen Q, Sundén B, et al. Parameter study of transient carbon deposition effect on the performance of a planar solid oxide fuel cell. APPL ENERG. 2015; 152:217-28.
11. Chen B, Xu H, Ni M. Modelling of finger-like channelled anode support for SOFCs application. SCI BULL. 2016; 61:1324-32.
12. Su S, Zhang Q, Gao X, Periasamy V, Kong W. Effects of changes in solid oxide fuel cell electrode thickness on ohmic and concentration polarizations. INT J HYDROGEN ENERG. 2016; 41:16181-90.
13. Wei SS, Wang TH, Wu JS. Numerical modeling of interconnect flow channel design and thermal stress analysis of a planar anode-supported solid oxide fuel cell stack. ENERGY. 2014; 69:553-61.
14. He Z, Birgersson E, Li H. Reduced non-isothermal model for the planar solid oxide fuel cell and stack. ENERGY. 2014; 70:478-92.
15. Yan M, Fu P, Li X, Zeng M, Wang Q. Mass transfer enhancement of a spiral-like interconnector for planar solid oxide fuel cells. APPL ENERG. 2015; 160:954-64.
16. Di Chu. Numerical Simulation of Electrochemical Properties of Plate Solid Oxide Fuel Cell: Institute of Scientific and Technical Information of China; 2020.
17. Hajimolana SA, Hussain MA, Daud WMAW, Soroush M, Shamiri A. Mathematical modeling of solid oxide fuel cells: A review. Renewable and Sustainable Energy Reviews. 2011; 15:1893-917.
18. Xiaolian Li. Optimization of interconnect structure of solid oxide fuel cell based on multi-physical modeling: Tsinghua University; 2018.
19. Kupecki J, Motylinski K, Milewski J. Dynamic analysis of direct internal reforming in a SOFC stack with electrolyte-supported cells using a quasi-1D model. APPL ENERG. 2018; 227:198-205.
20. Lin B, Shi Y, Cai N. Numerical simulation of cell-to-cell performance variation within a syngas-fuelled planar solid oxide fuel cell stack. APPL THERM ENG. 2017; 114:653-62.
21. Gawel DA, Pharoah JG, Beale SB. Development of a SOFC performance model to analyze the powder to

power performance of electrode microstructures. ECS Transactions. 2015; 68:1979.

22. Changfu Guo. Modeling Study on Transport Characteristics and Performance of Solid Oxide Fuel Cells: Dalian University of Technology; 2018.
23. Cui Y, Liu H, Wang Q, Zheng Z, Wang H, Yue Z, et al. Investigation on the ignition delay prediction model of multi-component surrogates based on back propagation (BP) neural network. COMBUST FLAME. 2022; 237:111852.